AIP | Applied Physics Letters

Optoelectronic behaviors and carrier dynamics of individual localized luminescent centers in InGaN quantum-well light emitting diodes

Suman De, Dibyendu Kumar Das, Arunasish Layek, Archana Raja, Manoj Kumar Singh et al.

Citation: Appl. Phys. Lett. **99**, 251911 (2011); doi: 10.1063/1.3671092
View online: http://dx.doi.org/10.1063/1.3671092
View Table of Contents: http://apl.aip.org/resource/1/APPLAB/v99/i25
Published by the American Institute of Physics.

Related Articles

Transport-mechanism analysis of the reverse leakage current in GaInN light-emitting diodes
Appl. Phys. Lett. 99, 253506 (2011)

Asymmetry of carrier transport leading to efficiency droop in GaInN based light-emitting diodes
Appl. Phys. Lett. 99, 251115 (2011)

Electroluminescence from Si nanocrystal/c-Si heterojunction light-emitting diodes
Appl. Phys. Lett. 99, 251113 (2011)

Diamond based light-emitting diode for visible single-photon emission at room temperature
Appl. Phys. Lett. 99, 251106 (2011)

Study of 375nm ultraviolet InGaN/AlGaN light-emitting diodes with heavily Si-doped GaN transition layer in growth mode, internal quantum efficiency, and device performance
J. Appl. Phys. 110, 123102 (2011)

Additional information on Appl. Phys. Lett.

Journal Homepage: http://apl.aip.org/
Journal Information: http://apl.aip.org/about/about_the_journal
Top downloads: http://apl.aip.org/features/most_downloaded
Information for Authors: http://apl.aip.org/authors

ADVERTISEMENT

Downloaded 23 Dec 2011 to 202.75.203.78. Redistribution subject to AIP license or copyright; see http://apl.aip.org/about/rights_and_permissions

Optoelectronic behaviors and carrier dynamics of individual localized luminescent centers in InGaN quantum-well light emitting diodes

Suman De,[1] Dibyendu Kumar Das,[2] Arunasish Layek,[1] Archana Raja,[1]
Manoj Kumar Singh,[3] Arnab Bhattacharya,[4] Subhabrata Dhar,[5] and Arindam Chowdhury[1,a)]
[1]*Department of Chemistry, Indian Institute of Technology Bombay, Powai, Mumbai 400076, India*
[2]*Department of Physical Chemistry, Indian Association for the Cultivation of Science, Jadavpur, Kolkata 700032, India*
[3]*Atomic & Molecular Physics Division, Bhabha Atomic Research Center, Trombay, Mumbai 400085, India*
[4]*Department of Condensed Matter Physics and Materials Science, Tata Institute of Fundamental Research, Homi Bhabha Road, Mumbai 400005, India*
[5]*Department of Physics, Indian Institute of Technology Bombay, Powai, Mumbai 400076, India*

(Received 11 July 2011; accepted 18 November 2011; published online 23 December 2011)

Spatially, spectrally, and temporally resolved photoluminescence (PL) microscopy was performed on InGaN quantum-well light emitting diodes to probe individual localized luminescent centers arising from disorder induced potential fluctuations. Two energetically distinct localization centers were identified where the photoemission quantum-efficiency (QE) are correlated to the transition energies. PL lifetime measurements on emission centers suggest that activation barrier for non-radiative recombination (NR) processes determines their QE. The disparity in carrier dynamics not only substantiate two diverse mechanisms for localization processes, but also indicate the presence of multiple NR channels even within the trap centers implying their lateral dimensions to span several nanometers. © *2011 American Institute of Physics*. [doi:10.1063/1.3671092]

The use of $In_xGa_{1-x}N$ based quantum-well (QW) heterostructures as active layers in solid-state light emitting diodes (LEDs) allows for tunability of photon energies from UV through visible spectral range.[1] Despite the large number ($\sim 10^9$–$10^{10}\,cm^{-2}$) of non-radiative recombination (NR) centers such as dislocations, the high photoemission quantum-efficiency (QE) of InGaN based LEDs is believed to be due to localization of carriers in radiative potential traps which abate NR processes.[2–5] Such modulation of the QW potential energy landscape has been ascribed to both compositional and interface morphology related disorders in the alloy layers.[3–8] Due to inhomogeneous nature of the radiative recombination (RR) centers, the optoelectronic behaviors of QWs vary considerably at the nanoscale, often manifested as spatially (in-plane) and energetically non-uniform light emission from QWs.[9,10] This is more apparent for blue and green emitting InGaN QWs, where low band-gap localized luminescent centers has been observed.[9–12] Further, anisotropy in the local nano-environment, i.e., the potential landscape surrounding each radiative trap center, has a tremendous impact on carrier dynamics and, as a consequence, on the QE of RR. It is, therefore, essential to understand the energetics and carrier recombination pathways in radiative traps due to carrier confinement. This can be achieved by interrogating individual spatially separated localized emission centers within an InGaN based LED in a non-invasive manner, such as using photoluminescence (PL). However, the excitation of barriers using high energy photons can be detrimental to selectively probe carrier dynamics within individual trap centers because the emanating luminescence is obscured by overwhelming RR though the entire alloy.

a)Author to whom correspondence should be addressed. Electronic mail: arindam@chem.iitb.ac.in. Tel.: +91 22 2576 7154.

Previously, two classes of localized emission centers within an InGaN based LED were identified in terms of their band-gap energies and RR efficiencies using spectrally resolved PL (SRPL) microscopy.[13] In this work, we have performed spatially and time-resolved PL (TRPL) imaging of InGaN QWs by selectively exciting the alloy layers, which allows us to probe carrier dynamics within individual localized luminescent centers.

The sample studied here is a green emitting multiple QW LED consisting of 4 nm $In_{0.22}Ga_{0.78}N$ wells separated by 10 nm GaN barriers, grown using metallorganic vapor phase epitaxy on a c-plane sapphire substrate. PL microscopy was performed using a 488 nm Ar^+ laser at 298 K. Energy-mapped images were obtained using green (530–590 nm) and red (590-700 nm) band-pass filters. Spatially resolved ($\sim$200 nm) and large area ($\sim 100\,\mu m^2$, $\lambda_{ex} = 405$ nm) PL spectra were obtained using an adjustable slit and transmission grating placed before the CCD detector. TRPL imaging was carried out in a scanning confocal microscope (SCM) using a 470 nm pulsed laser with 250 ps pulse-width and 40 MHz repetition rate, at 1 kW/cm^2. The PL decay was recorded via time-correlated single-photon counting using an avalanche photodiode. For details, see Ref. 13 and supporting information.[20]

An energy-mapped (pseudo-color) PL intensity image of the QWs (Figure 1(a)) shows the presence of highly localized (diffraction-limited) luminescent centers (or "dots"). Detection of dots through both the lower-energy (as compared to QWs) emission channels reveals that these are radiative potential traps which funnel carriers efficiently. Characteristic PL emission spectra of five individual dots along with the large-area PL spectrum of the QWs are shown in Figure 1(b). The large-area PL spectrum is dominated by a transition at $\sim$2.6 eV (regarded as the QW band-gap), along with a broad yellow luminescence band, which

 © 2011 American Institute of Physics

Downloaded 23 Dec 2011 to 202.75.203.78. Redistribution subject to AIP license or copyright; see http://apl.aip.org/about/rights_and_permissions

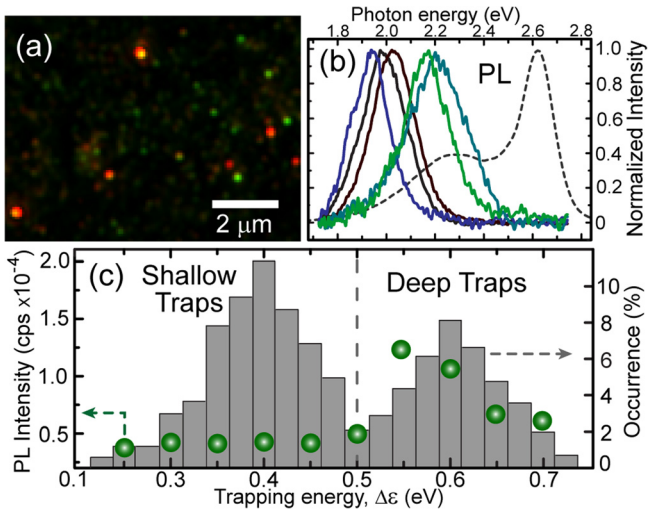

FIG. 1. (Color online) (a) Semi-quantitative energy-mapped PL image of QWs. (b) Single-dot (solid lines, $\lambda_{ex} = 488$ nm) and large-area (dashed line, $\lambda_{ex} = 405$ nm) PL emission spectra. (c) Distribution of $\Delta\varepsilon$ (bars) and the average intensities (spheres, 50 meV bins) plotted as a function of $\Delta\varepsilon$.

originates from defect states of GaN barrier layer as confirmed by PL spectra of a reference GaN sample. Single-dot spectra demonstrate that individual traps have transition energies down to ~1.9 eV, i.e., ~750 meV lower than that of the alloy. A frequency distribution of relative *lowering* of transition energies ($\Delta\varepsilon$) due to trap formation, generated from 1100 single-dot PL spectra, is shown in Figure 1(c). Intriguingly, this distribution is found to be bimodal in nature (minima at ~2.1 eV), which implies that band-gaps associated with radiative centers lie within two well-separated (~200 meV) energetic domains, classified as shallow ($\Delta\varepsilon^S < \sim 480$ meV) and deep ($\Delta\varepsilon^D > \sim 500$ meV) traps. The variation of average PL intensities of dots with $\Delta\varepsilon$ (Figure 1(c)) is consistent with Figure 1(a); majority of shallow traps are relatively weak emitters, while almost all the efficient luminescent centers are deep traps.

A SCM image of the QWs obtained using the two detection channels, and the corresponding TRPL image is shown in Figure 2. The pseudo-color PL intensity image (Figure 2(a)) is used to identify the shallow and deep traps. From Figure 2(b), it is clear that the average PL lifetimes (τ_{av}) for red dots (~6 ns) are consistently higher than the green dots (~2 ns), while τ_{av} of the QW background is much lower (<0.5 ns). Figure 2(c) shows the typical distribution of single-dot PL lifetimes, as obtained by analyzing PL decay traces collected over several minutes.[20] Importantly, the spread of the lifetime distributions for shallow traps is always found to be more than that of deep traps. The width of these statistically relevant PL lifetime distributions is a direct measure of the heterogeneity in carrier recombination pathways inside each dot.[14] This suggests that the number of RR and/or NR pathways accessed by carriers within shallow traps is significantly higher than those available within deep traps.

Figure 3 shows characteristic time-resolved PL traces, depicting the range of observed decay dynamics for individual shallow and deep traps. Consistent with TRPL images, the PL decay for the shallow traps are found to be faster than the deep traps. Neither of these TRPL traces could be fit

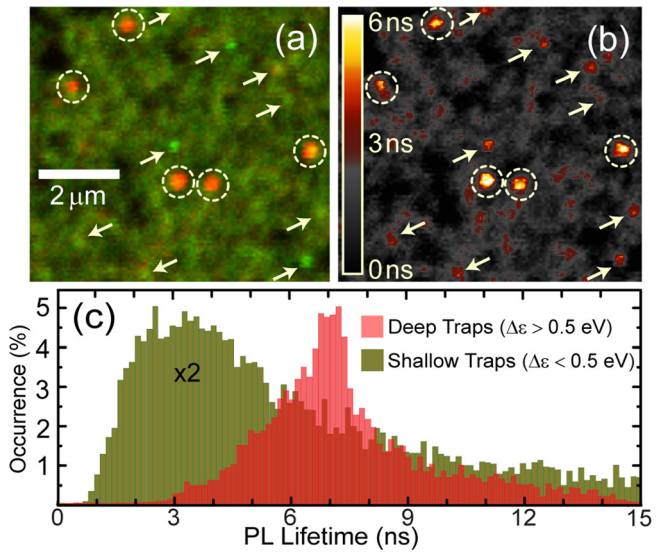

FIG. 2. (Color online) (a) Energy-mapped SCM intensity image showing green (arrows) and red (circles) emitting dots. (b) PL lifetime image of the same area, where τ_{av} in each pixel is color-coded. (c) PL lifetime distribution for a single shallow and deep trap.

using a single-exponential decay. However, a bi-exponential function yielded excellent fits for all dots irrespective of their $\Delta\varepsilon$. For shallow traps, the fast component ($\tau_1^S \sim 0.4$ ns) has a dominant contribution (90%) as compared to the slow one ($\tau_2^S \sim 4$ ns). In contrast, both fast ($\tau_1^D \sim 1$ ns) and slow ($\tau_2^D \sim 6$ ns) components have comparable contributions for the deep-traps.

The carrier dynamics within potential traps in InGaN alloy is governed by two competing processes: (1) RR of carriers within the traps, which primarily depends upon the overlap of electron-hole wavefunctions and (2) non-radiative escape from the potential wells where they are confined. Strong carrier localization in traps reduces access to non-radiative pathways due to the restriction of carrier movement. At room temperature, however, the thermal escape of carriers to NR centers is considerably faster than RR processes.[15–17] Therefore, the fast (τ_1) component of the observed TRPL traces are attributed primarily to carrier escape to NR centers (τ_{NR}), while the slow component (τ_2) is assigned as predominantly due to RR within the traps (τ_{RR}). Our results show that the rate of NR (k_{NR}) is high for shallow

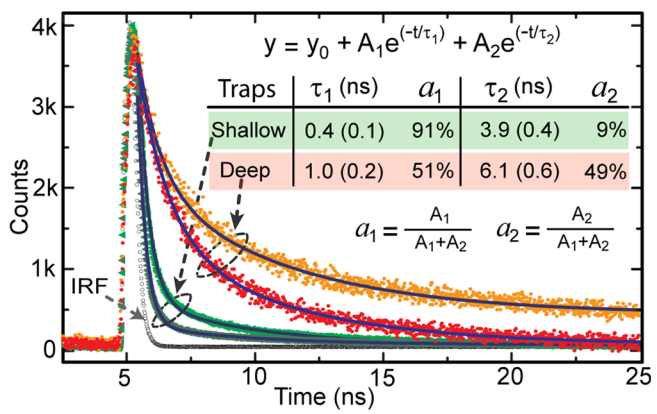

FIG. 3. (Color online) Single-dot TRPL traces (symbols) and fits (lines). Decay parameters tabulated in inset. IRF is instrument response function.

Downloaded 23 Dec 2011 to 202.75.203.78. Redistribution subject to AIP license or copyright; see http://apl.aip.org/about/rights_and_permissions

traps, where majority (90%) of carriers can easily access the NR centers. However, k_{NR} as well as number of available NR pathways decrease considerably for deep traps.

Considering that carriers trapped in these localization centers require an activation energy (Δ) to access NR pathways, carrier dynamics will be governed by $dn_1/dt = -k_{NR}n_1$ and $dn_2/dt = -k_{RR}n_2$, where k_{RR} is rate of RR, while n_1 and n_2 are the number of activated carries which escape to NR centers and those which undergo RR in the potential trap, respectively, such that $n_1 = (n_1 + n_2)\exp(-\Delta/k_BT)$.[18] Note that n_2/n_1 is equal to the ratio of pre-exponential coefficients (a_2/a_1) evaluated from the fit to TRPL decay (Figure 3). Therefore, Δ can be expressed as $\Delta = k_BT\ln(1 + a_2/a_1)$, and the QE for RR as $\eta = a_2k_{RR}/(a_1k_{NR} + a_2k_{RR})$. For the shallow and deep traps, we estimate $\Delta_S \sim 3$ meV and $\Delta_D \sim 18$ meV, while $\eta_S \sim 0.01$ and $\eta_D \sim 0.14$ (subscripts S/D refer to shallow/deep traps). The enhancement of η for deep traps is found to be consistent with the average PL intensities observed for individual dots (Figure 1). Interestingly, however, both Δ_S and Δ_D are significantly lower than the individual potential well-depths (150–300 meV). This implies that photogenerated carriers present within both the shallow and deep traps can access NR pathways even without escaping from the potential wells. This is possible only if the localization centers span few tens of nanometers in lateral dimension in order to accommodate several NR centers such as dislocations. This in concurrence with a recent report on the presence of multiple V-shape pits (NR centers) inside red-shifted localization centers within InGaN QWs.[19] Under these premises, the carrier dynamics within individual traps formed within QWs are schematically depicted in Figure 4. Depending on the number of NR sites present within each emission center, as well as the energetic barriers surrounding these NR sites, the relative QEs of individual dots vary. The shallow-traps have more number of available NR channels (evident from Figure 2(c)) and lower activation energy to surpass in order to access these NR centers, resulting in lower QEs of photoemission as compared to the deep traps.

The clear bimodal distribution of transition energies coupled with an abrupt increase in emission intensities for traps having $\Delta\varepsilon > 500$ meV (Figure 1(c)) is indicative of their diverse origins. It is also evident that carrier dynamics occurring within the shallow traps is very different from those of deep traps, ensuing in considerable disparity in their QEs. Both in-plane fluctuations in QW thickness and local In compositions can spatially confine carriers and thereby result in highly luminescent radiative traps.[3,4,7] However, it is unlikely that non-uniform changes of either of these parameters results in a bimodal distribution of $\Delta\varepsilon$ and RR efficiencies accompanied by contrasting carrier dynamics.[13] Therefore, single-dot TRPL measurements further substantiate the presence of two very distinct carrier localization centers, the optoelectronic properties of which are dictated by the depth and width of individual traps as well as on the local potential landscape. Indeed, activation barriers to access NR pathways can differ considerably for the deep and shallow traps, depending on the local strain energies of individual localization centers.[19] The local strain is extremely sensitive to In mole-fractions in the vicinity of NR centers, resulting in higher barriers for In-rich localization centers which act as deep traps.

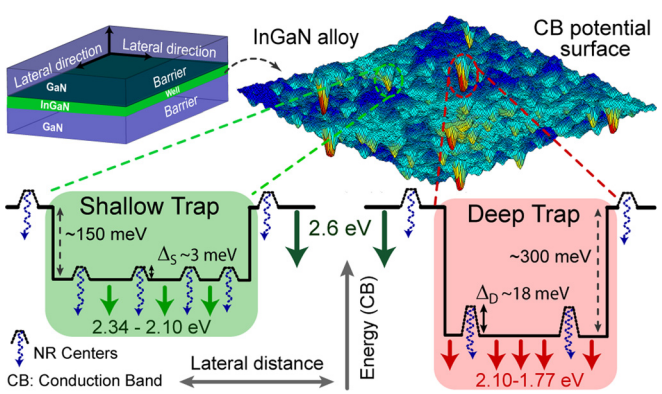

FIG. 4. (Color online) Model depicting potential energy surface of the alloy layer and carrier recombination processes in shallow and deep traps.

In summary, we establish the presence of two distinct categories of localization centers within the same InGaN QW-LED, where carrier recombination dynamics is very different, correlated to their transition energies. A higher rate and enhanced probability of non-radiative escape within the shallow traps, likely due to significant heterogeneity present therein, render carriers more susceptible to non-radiative deactivation culminating in reduced QEs. In contrast, deep traps abate carrier migration to nearby dislocations due to the presence of higher activation barriers, allowing these to be more efficient. Single-dot TRPL shows that NR centers can be accessed even within each localization center, implying their spatial dimensions to be several nanometers at the least. Control over the underlying physical parameters responsible for such remarkably dissimilar optoelectronic properties in these two classes of localization centers can be beneficial in fabricating lower energy and higher efficiency InGaN based optoelectronic devices.

We acknowledge K. Bhattacharyya for the usage of DST (IRPHA), India, funded Centre for Ultrafast Spectroscopy and Microscopy, A. Datta for valuable discussions, IIT-Bombay and CSIR (India) for research grants to A.C and PhD fellowships to A.L. and S.D.

[1]S. Nakamura and S. F. Chichibu, *Introduction to Nitride Semiconductor Blue Lasers and Light Emitting-Diodes* (Taylor & Fancis, New York, 2000).
[2]S. Nakamura, Science **281**, 956 (1998).
[3]S. Chichibu, T. Azuhata, T. Sota, and S. Nakamura, Appl. Phys. Lett. **69**, 4188 (1996).
[4]D. M. Graham, A. Soltani-Vala, P. Dawson, M. J. Godfrey, T. M. Smeeton, J. S. Barnard, M. J. Kappers, C. J. Humphreys, and E. J. Thrush, J. Appl. Phys. **97**, 103508 (2005).
[5]Y. Narukawa, Y. Kawakami, M. Funato, S. Fujita, S. Fujita, and S. Nakamura, Appl. Phys. Lett. **70**, 981 (1997).
[6]S. Dhar, U. Jahn, O. Brandt, P. Waltereit, and K. Ploog, Phys. Status Solidi A **192**, 85 (2002).
[7]M. J. Galtrey, R. A. Oliver, M. J. Kappers, C. J. Humphreys, P. H. Clifton, D. Larson, D. W. Saxey, and A. Cerezo, J. Appl. Phys. **104**, 013524 (2008).
[8]C. Karcher, K. Jandieri, B. Kunert, R. Fritz, M. Zimprich, K. Volz, W. Stolz, F. Gebhard, S. D. Baranovskii, and W. Heimbrodt, Phys. Rev. B **82**, 245309 (2010).
[9]K. Okamoto, A. Kaneta, Y. Kawakami, S. Fujita, J. Choi, M. Terazima, and T. Mukai, J. Appl. Phys. **98**, 064503 (2005).
[10]H. Schomig, S. Halm, A. Forchel, G. Bacher, J. Off, and F. Scholz, Phys. Rev. Lett. **92**, 106802 (2004).
[11]S. Chichibu, K. Wada, and S. Nakamura, Appl. Phys. Lett. **71**, 2346 (1997).

Downloaded 23 Dec 2011 to 202.75.203.78. Redistribution subject to AIP license or copyright; see http://apl.aip.org/about/rights_and_permissions

[12]M. G. Cheong, C. Liu, H. W. Choi, B. K. Lee, E. K. Suh, and H. J. Lee, J. Appl. Phys. **93**, 4691 (2003).
[13]S. De, A. Layek, A. Raja, A. Kadir, M. R. Gokhale, A. Bhattacharya, S. Dhar, and A. Chowdhury, Adv. Funct. Mater. **21**, 3828 (2011).
[14]C. Eggeling, J. R. Fries, L. Brand, R. Gunther, and C. A. M. Seidel, Proc. Natl. Acad. Sci. U.S.A. **95**, 1556 (1998).
[15]Y. Narukawa, Y. Kawakami, S. Fujita, and S. Nakamura, Phys. Rev. B **59**, 10283 (1999).
[16]C. Netzel, V. Hoffmann, T. Wernicke, A. Knauer, M. Weyers, M. Kneissl, and N. Szabo, J. Appl. Phys. **107**, 033510 (2010).
[17]T. Li, A. M. Fischer, Q. Y. Wei, F. A. Ponce, T. Detchprohm, and C. Wetzel, Appl. Phys. Lett. **96**, 031906 (2010).
[18]It has been considered that carriers are always in thermal equilibrium within the localization centers, and therefore, the coupling between n_1 and n_2 can be neglected. k_B is Boltzmann constant.
[19]J. Bruckbauer, P. R. Edwards, T. Wang, and R. W. Martin, Appl. Phys. Lett. **98**, 141908 (2011).
[20]See supplementary material at http://dx.doi.org/10.1063/1.3671092 for detail description of experimental techniques and data analyses procedures.

Downloaded 23 Dec 2011 to 202.75.203.78. Redistribution subject to AIP license or copyright; see http://apl.aip.org/about/rights_and_permissions

Supplementary Information

Insight on optoelectronic behaviors and carrier dynamics of individual localized luminescent centers within InGaN/GaN quantum-well light emitting diodes

Suman De[1], Dibyendu Kumar Das[3], Arunasish Layek[1], Archana Raja[1], Manoj Kumar Singh[4], Arnab Bhattacharyya[5], Subhabrata Dhar[2] and Arindam Chowdhury[1]*

[1]Department of Chemistry and [2]Department of Physics, Indian Institute of Technology-Bombay, Powai, Mumbai 400076, India; [3]Department of Physical Chemistry, Indian Association for the Cultivation of Science, Jadavpur, Kolkata 700032, India; [4]Atomic & Molecular Physics Division, Bhabha Atomic Research Center, Trombay, Mumbai 400085, India; [5]Department of Condensed Matter Physics and Materials Science, Tata Institute of Fundamental Research, Homi Bhaba Road, Mumbai 400005, India

The InGaN quantum well (QW) light emitting diode (LED) structures were grown on c-plane sapphire substrates using metalorganic vapor phase epitaxy (MOVPE) in a 3x2 inch close coupled showerhead reactor. The active region consists of a 5 QW stack with InGaN quantum wells separated by lightly n-doped GaN barrier layers. A standard two-temperature growth process under nitrogen carrier gas is used for the growth of the active region, with the InGaN QW grown at a lower temperature (660 ^{o}C) than the GaN barrier (720 ^{o}C) to enhance the Indium incorporation in the QW. Structural characterization using high-resolution X-ray diffraction shows distinct superlattice fringes; simulation of the diffraction profiles for multiple reflections is used to estimate the average layer thickness and Indium content. From the x-ray data we estimate the active region to have ~4 nm thick wells having ~22% average Indium composition, separated by ~10 nm thick GaN barrier layers. Electroluminescence spectra obtained from different regions of the wafer showed that this is a functional "green" LED.

The 488 nm line of an Ar+ laser (Mellos Griot) was used to selectively excite the $In_{0.22}Ga_{0.78}N$ QW in epi-fluorescence configuration through an inverted microscope (Nikon Eclipse 2000U) using 60X 1.49NA oil immersion objective lens (Nikon). The PL emission was collected using the same objective lens and separated from the excitation beam by using a dichroic mirror (Semrock – Di01-R488) and a 488 nm notch filter (NF03-488E-25) and subsequently imaged using cooled CCD (charged couple device) camera (DVC-1412AM) at 100ms exposure times. Dual-color imaging was performed by collecting the emission using two bandpass filters (from Semrock): green-yellow (530-590 nm) and orange-red (590-700 nm). High-throughput PL emission profiles of individual Dots were obtained by collecting the emission through a combination of adjustable slit and transmission grating (70 lines/mm, Optometrics) mounted in front of the CCD. Spectral positions were calibrated using four laser wavelengths (488, 514.5, 532 and 633 nm). All data were obtained at identical excitation powers of ~500W/cm^2 at 295K.

All the microscopy images were analyzed after background flattening due to slight modulations in the excitation field unless otherwise mentioned. For band-gap mapping, individual images of the same lateral area obtained in the two detection channels were quantitatively overlaid to generate a pseudo-color energy mapped image (using ImageJ, NIH). As a qualitative indicator of optical band-gaps for individual Dots, the higher and lower energy detection channels have been assigned green and red colors. The spectrally resolved images were analyzed after appropriate background subtraction and corrected for the CCD detector response over the entire wavelength range. The emission spectrum obtained for each spatially separated diffraction-limited spot was fitted to a single Gaussian to obtain their spectral maxima positions (λ_{max}^{em}) and integrated intensities. Meticulous care was taken for estimation of λ_{max}^{em} for all the spatially well-separated (>200 nm) individual spots resulting in a wavelength resolution of ~2.5 nm. The band-gaps of individual Dots were directly obtained from the transition energies (ν_{max}^{em}) while the integrated intensities for all the ~1100 randomly chosen Dots were obtained by integrating the emission spectral profiles. The frequency histogram shown in Figure 1 (c) was constructed at 25 meV bins, while average intensities over 50 meV bins were plotted against the corresponding band-gaps of Dots. For further details on the experimental setup, see Ref.13.

Fluorescence Lifetime Imaging Microscopy (FLIM) studies were carried out in a confocal laser scanning microscopy (CLSM) setup (PicoQuant, MicroTime 200) using an inverted optical microscope (Olympus IX-71). A water immersion objective (60×1.2 NA) was used to focus the excitation light of 470 nm with repetition rate of 40 MHz, from a pulsed diode laser (PDL 828-S "SEPIA II", PicoQuant) providing 10–20 μW power on to the sample. The photoluminescence was collected in an epifluorescence configuration and allowed to pass through a dichroic mirror and appropriate band pass filters. For collecting the lifetime decay of individual Dots, the PL

emission signal was focused through a pinhole (50 μm) onto single-photon counting avalanche photodiode (SPAD). All the data collection and fitting were performed in Symphotime software. It should be noted that Figure 2(a) is not a quantitative energy-mapped intensity image, but rather a qualitative pseudo-color image obtained by collecting the emission (of the same lateral area) using the green (530-590 nm) and red (590-700 nm) bandpass filters. The resulting images from individual channels were merged to obtain the qualitative color image, which was used to identify the shallow and deep traps. However, the FLIM image (of the same area as in Figure 2(a)) shown in Figure 2 (b) was obtained using the same LSCM setup by collecting the emission without the use of bandpass filters. PL lifetime of individual diffraction-limited spots from the image has been obtained using time correlated single photon counting (TCSPC) which ensures a high temporal resolution at enhanced sensitivity. Multi-exponential fit was applied to the image (pixel by pixel) to construct the lifetime image. PL lifetime fitting has been done using iterative convolution, taking into account the influence of the instrument response function (IRF). False color lifetime image was constructed to maximize the amount of information presented in the display of the results, which was exported directly as ASCII files for subsequent data analysis. The average lifetime (τ_{av}) of an emissive trap has been calculated using the expression $\tau_{av} = \left(a_1\tau_1^2 + a_2\tau_2^2 / a_1\tau_1 + a_2\tau_2\right)$ following *Principal of Fluorescence Spectroscopy, Joseph R. Lackowicz, 3rd edition, Springer*. In the lifetime image contrast and brightness are adjusted to exemplify the both bright and dim spots. PL lifetime distributions are obtained by plotting the lifetime of an individual diffraction-limited spot against acquisition time (Figure S1). The PL lifetime decay of each spot has been averaged over 1 ms, which constitute a single data point in the histogram generated in Figure 2(c) and Figure S1. A reliable PL lifetime distribution histogram has been constructed by collecting data over tens of seconds. For further details on the procedure, see Ref. 14 of the main text.

Figure S1. The PL lifetimes traces of shallow (bottom panel) and deep traps (top panel) plotted against acquisition time. The corresponding projections in the y-axis show the histogram of average PL lifetimes obtained for data acquired during 200 ms.

Supplementary Figure: